Atmospheric Research 237 (2020) 104838

Contents lists available at ScienceDirect

Atmospheric Research

journal homepage: www.elsevier.com/locate/atmosres

Characterizing atmospheric controls on winter urban pollution in a topographic basin setting using Radon-222

Dafina Kikaj[a,b], Scott D. Chambers[c], Matjaž Kobal[d], Jagoda Crawford[c], Janja Vaupotič[b,*]

[a] Jožef Stefan International Postgraduate School, Jamova cesta 39, 1000 Ljubljana, Slovenia
[b] Jožef Stefan Institute, Department of Environmental Sciences, Jamova cesta 39, 1000 Ljubljana, Slovenia
[c] ANSTO, Environmental Research, Locked Bag 2001, Kirrawee DC, NSW 2232, Australia
[d] Aerosol d.o.o. Kamniška ulica 39A, 1000 Ljubljana, Slovenia

ARTICLE INFO

Keywords:
Radon
Stability
Persistent temperature inversion
Complex topography
Urban pollution

ABSTRACT

Using hourly meteorological, air quality and radon observations over two winters (2016–2017 and 2017–2018), we combine diurnal and synoptic timescale radon-based mixing classification techniques, for the first time, to better understand air quality variability in the sub-Alpine city of Ljubljana. Of the two winters, only the second experienced significant snow cover (> 1 month). A total of six mixing classes were defined for each winter: 5 diurnal and 1 synoptic ("persistent temperature inversion", PTI); the latter being internally categorised as "strong" or "weak". Diurnal and synoptic changes in mixing state played an important role in air quality variability in both winters. Little diurnal accumulation of local pollutants (CO, NO_2, PM_{10} and BC) was observed for wind speeds ≥ 1.5 m s^{-1} (mixing classes #1 to #3). Under these windy conditions significant remote contributions to SO_2 and O_3 concentrations in Ljubljana were observed, primarily from the Po Valley region. The most stable conditions (class #5 and PTI days), characterized by nocturnal wind speeds ≤ 0.5 m s^{-1} or rates of 2 m air temperature change ≥ 1.5 °C h^{-1}, were associated with the worst air quality conditions. Only under class #5 and PTI conditions did daily-mean PM_{10} concentrations exceed both EU and WHO guideline values. The absence of snow cover in the first winter resulted in stronger thermodynamic stability and higher pollution concentrations. Other contributing factors included a 28% larger traffic source near the monitoring site and a 17% greater consumption of heating fuel that winter in Ljubljana.

1. Introduction

The rapid growth of urbanization, vehicle numbers, energy consumption, and industrialization throughout Europe has degraded urban air quality (Karanasiou and Mihalopoulos, 2013; EEA, 2018). Most pollutants are emitted directly into the atmospheric boundary layer (ABL) from surface-based sources, or formed there as a result of precursor reactions. Since commuters and urban buildings primarily inhabit the lower ~10% of the ABL, air pollution has become a major cause of diseases and premature deaths (Pope and Dockery, 2006; Goudie, 2014). Consequently, the World Health Organization (WHO) and European Union (EU) have recommended limits for "criteria pollutant" concentrations based on short-term ($\leq$24-h) and long-term (annual) exposure periods. Despite recent improvements in some aspects of air quality (e.g. sulphur dioxide, SO_2, and carbon monoxide, CO, levels; EEA, 2016, 2017, 2018), non-compliance with air quality guidelines values for some species is still reported in many parts of Europe, especially in the Mediterranean Basin Region (MBR). In particular, target limits for nitrogen dioxide (NO_2), particulate matter (PM) and tropospheric ozone (O_3) are frequently exceeded in the MBR (EEA, 2017, 2018). However, the levels of some pollutants (e.g. black carbon; BC) are not yet regulated by the WHO or EU, despite exposure to even small concentrations of BC having been linked with cardiorespiratory diseases (Janssen et al., 2011; Dons et al., 2012).

Since urban pollution scales with population (Ayers et al., 1982), and the size and population of urban regions is continually increasing, it will be important to continually review target limits and assess the efficacy of mitigation measures. The ability to do so effectively will rely upon understanding controls on pollutant concentration variability near the surface in the "zone of habitation". In this regard, it is important to recognise that pollution concentrations vary according to both "controllable" and "uncontrollable" influences. The ability to distinguish between these influences will be crucial to more accurately assessing the efficacy of mitigation measures.

* Corresponding author.
E-mail address: janja.vaupotic@ijs.si (J. Vaupotič).

https://doi.org/10.1016/j.atmosres.2019.104838
Received 15 August 2019; Received in revised form 22 December 2019; Accepted 26 December 2019
Available online 27 December 2019

"Controllable" influences, the target of mitigation measures, relate to matters directly affecting pollution source strengths and their spatial and temporal variability. "Uncontrollable" influences, on the other hand, include: meteorology, geographic setting and topographic effects, and cross-boundary (remote) pollution transport. Diurnal timescale changes in the ABL mixing state ("stability"), associated with daytime convection and the formation of nocturnal inversion layers, are known to influence pollution concentrations (Chambers et al., 2015; Wang et al., 2016; Williams et al., 2016). Furthermore, in regions of complex topography such as basin or steep valley environments, longer timescale (e.g. synoptic) changes in the ABL mixing state can also occur. The most severe examples are persistent temperature inversions (PTIs) typically occur in winter months, when days are short and persistent snow-cover limits the extent of daytime convection, under regional subsidence (anticyclonic) conditions, which further retard dispersion and lead to pollution events of potentially life-threatening duration and intensity (Wang et al., 2019; Rakovec et al., 2002, 2015; Silcox et al., 2012; Whiteman et al., 2014; Largeron and Staquet, 2016; Baasandorj et al., 2017; Kikaj et al., 2019a). In Europe, where political boundaries can be very close, another form of synoptic-timescale variability of urban pollution arises through cross-boundary advection events from regions whose land-use practices and emissions policies are beyond the influence of local government mitigation efforts (Kallos et al., 2006; Poberžnik and Štrumbelj, 2016; Chambers et al., 2016a; Chambers et al., 2017; He et al., 2018).

It has been well-established that near-surface atmospheric radon (^{222}Rn or radon-progeny) measurements are a powerful indicator of diurnal mixing and synoptic-timescale transport in the ABL, largely attributable to radon's ubiquitous nature and unique combination of physical characteristics (Allegrini et al., 1994; Perrino et al., 2001; Sesana et al., 2003; Zahorowski et al., 2004; Williams et al., 2013; Kikaj et al., 2019a). Furthermore, in many situations radon-based atmospheric stability classification provides a simpler, more consistent and representative indication of the nocturnal or daytime mean atmospheric mixing state than conventional meteorological approaches (Bowen, 1994; Chambers et al., 2015, 2019a; Crawford et al., 2016; Kahl and Chapman, 2018).

Vertical radon gradients provide the most direct evidence of the integrated effects of diurnal timescale near-surface mixing processes since they automatically account for air mass fetch effects (Moses et al., 1960; Cohen et al., 1972; Porstendörfer et al., 1991; Chambers et al., 2011; Williams et al., 2011). Such measurements, however, have very stringent requirements on instrument performance. Single-height near-surface radon measurements, on the other hand, can be used to provide a good approximation of vertical radon gradient observations for diurnal timescale ABL mixing studies (Chambers et al., 2015; Williams et al., 2016), with more relaxed measurement requirements. In fact, at sites sufficiently removed from coastal influences (i.e. by at least 10–20 km), near-surface radon concentrations are often high enough to be measured with portable, inexpensive instruments (e.g. Chambers et al., 2016b). However, a fundamental assumption of both of these approaches is that changes in the atmospheric mixing state do not contribute to observed radon concentration variability on greater than diurnal timescales. In complex terrain under PTI conditions this assumption is clearly violated, since the basin atmosphere stagnates for several days, allowing radon to accumulate between the surface and synoptic inversion. Under these conditions a shallow stable nocturnal boundary layer may also develop, but it would be weaker than if the overlying persistent synoptic inversion was not present. When this surface inversion breaks down the following morning, it mixes with the already high-radon air beneath the persistent synoptic inversion. In these situations, if "fetch effects" are removed as described by Chambers et al. (2015), the multi-day accumulation of radon under the synoptic inversion is incorrectly removed as a "fetch effect", and the affected measurement days are incorrectly assigned to an intermediate stability class due to weaker surface inversion conditions. In regions prone to the development of PTI conditions it is therefore necessary to identify synoptic timescale PTI conditions separately to the classification of diurnal timescale changes in the atmospheric mixing state. To this end, several approaches for PTI identification have been discussed in the literature (Largeron and Staquet, 2016; Fiorella et al., 2018; Kikaj et al., 2019a).

The primary objective of this study is to combine, for the first time, new (Kikaj et al., 2019a) and existing (e.g. Chambers et al., 2019a, and references therein) radon-based methods of atmospheric stability classification to separately characterize local influences on urban pollution variability in the Ljubljana Basin region on diurnal and synoptic timescales, as well as remote contributions to pollution on synoptic timescales. The statistics based on each of the defined mixing states, with well-defined occurrence frequencies, are used to inform upon potential health effects within the Ljubljana Basin compared with existing WHO and EU guideline values. Robust pollution statistics derived for only the most stable nocturnal mixing conditions, when atmospheric mixing depths are most well-constrained, will provide a benchmark against which future values can be compared to test the efficacy of mitigation measures.

Our study focuses only on winter months (December–February), the time of most frequent pollution exceedance events, due to the typically high rates of energy consumption (Energy Balance of City of Ljubljana, Final Report, City of Ljubljana, 2018) and frequent occurrence of PTIs in the Ljubljana Basin (Petkovšek, 1985, 1992; Rakovec et al., 2002; Kikaj et al., 2019a). Two winter periods of contrasting permanent snow cover are compared. Our results will summarize progress on the following specific tasks: (i) estimating nocturnal and forecasting daytime stability classes for whole 24-h periods across two winters (2016–2017 and 2017–2018) (Section 2.3); (ii) identifying synoptic timescale persistent temperature inversion events to extend the daily stability classifications of (i) from 5 to 6 classes (Section 2.3); (iii) characterizing meteorological conditions across the diurnal cycle for each of the six 24-h atmospheric stability classes (Section 3.1); (iv) characterizing the concentration variability of selected urban pollutants across the diurnal cycle for each of the mixing classes (Section 3.3); (v) constraining remote contributions to pollution variability in the Ljubljana Basin under conditions of strong advection (Section 3.4); and (vi) comparing extremes of pollution variability to WHO and EU guideline values (Section 3.5).

2. Methods

Hourly air quality, meteorology and atmospheric radon concentration (^{222}Rn) were monitored during the winters of 2016–2017 (W_{16-17}) and 2017–2018 (W_{17-18}) at a sub-Alpine Basin site (SAB; Ljubljana Bežigrad; Fig. 1b), in the central part of Ljubljana city, considered to be an urban background site (Titos et al., 2015; Gjerek et al., 2016; Pucer and Štrumbelj, 2018).

2.1. Site and surrounds

Ljubljana (299 m above sea level, a.s.l.), the capital of Slovenia, is a city of modest size (~280,000 inhabitants) situated in a sub-Alpine basin. The SAB site is surrounded by peaks of the Julian, Kamnik-Savinje, and Dinaric Alps reaching elevations of ~1000 m (Vrhovec, 1990; Hitzenberger et al., 2006). The complexity of the topography surrounding the basin retards synoptic winds, resulting in mean winter wind speeds of 1.3 m s^{-1} with frequent periods of PTI (33% of the year; ARSO, 2017). The PTI periods are characterized by foggy days favouring the build-up of locally-sourced emissions (Kikaj et al., 2019a).

Air quality within Ljubljana Basin is influenced by a combination of local and remote sources, the relative contributions of which depend on the prevailing meteorology. Since there are no large industries in city, the dominant local source of pollution is traffic; as well as domestic heating in the colder months, which has increased by 17% in the last

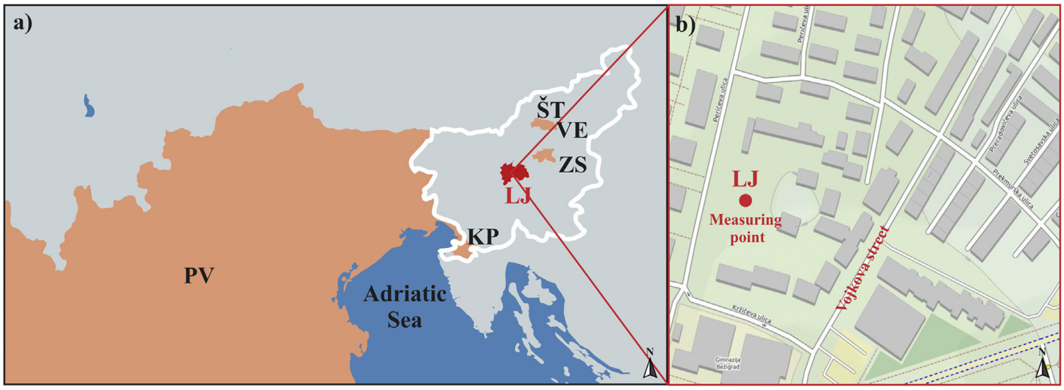

Fig. 1. a) Location of Ljubljana (LJ) within the most industrialized sites around (shaded area, Po Valley-PV, Port of Koper-KP, Zasavje-ZS, Šoštanj-ŠT and Velenje-VE), and b) close-up of Ljubljana city, showing the location of monitoring point (radon, meteorological and air quality data), the nearest street (Vojkova) with modest traffic. *Basemap source: © OpenStreetMap and mapchart.*

2 years (2016–2018) (Energy Balance of City of Ljubljana, Final Report, City of Ljubljana, 2018). For $W_{16–17}$ an overall higher consumption of fuels was noted, mostly due to the lower air temperatures during the heating season (Energy Balance of City of Ljubljana, Final Report, City of Ljubljana, 2018). In contrast to $W_{16–17}$, the next winter ($W_{17–18}$) was characterized by higher air temperatures and 31 days of snow cover. In the city, the Toplarna thermal power plant is located 3 km ESE of the SAB monitoring site. In Ljubljana, road maintenance and detours significantly reduced traffic flow in $W_{17–18}$ compared with $W_{16–17}$, including the number of vehicles passing through Vojkova Street (closest to the measuring point, Fig. 1b). On average, there were 8128 vehicles per day on Vojkova Street in $W_{16–17}$, compared with 6329 in $W_{17–18}$.

In terms of remote pollution sources, due its location the Ljubljana Basin serves as a "crossroads" for polluted air masses originating from: Africa (Kallos et al., 2006); across Europe from the North Atlantic Ocean and across Italy from the Mediterranean Sea (He et al., 2018); the northern Balkan Peninsula, and Eastern Europe (Poberžnik and Štrumbelj, 2016; He et al., 2018). Specifically, the heavily industrialized Po Valley region of Northern Italy (Bigi et al., 2017) and the shipping emissions (Slovenian seaport-Port of the Koper) lies 335 km and 60 km WSW, respectively, of Ljubljana city, while the Zasavje region with coal mines and various kinds of heavy industry (Lafarge Cement plant, Steklarna Hrastnik glass production, IGM Zagaroje building material company) lies 37 km to the NE, and Velenje town with Slovenia's largest lignite-thermal power plant-Šoštanj lies 56 km to the NE (see Fig. 1a) (Gjerek et al., 2016; Gjerek et al., 2017; He et al., 2018; Pucer and Štrumbelj, 2018).

2.2. Air quality and meteorology observations

Air quality parameters including particulate matter of median aerodynamic diameter ≤ 10 µm (PM_{10}), carbon monoxide (CO), nitrogen dioxide (NO_2), sulphur dioxide (SO_2), and ozone (O_3), were provided by the National Meteorological Service at the Slovenian Environmental Agency (ARSO). PM_{10} concentrations were measured with a continuous direct mass measurement for particulate matter utilizing a tapered element oscillating microbalance (TEOM). NO_2 was measured with chemiluminescence, SO_2 with ultraviolet fluorescence, and O_3 with ultraviolet photometry (Gjerek et al., 2017). In addition, black carbon (BC) was measured with a Magee Scientific Aethalometer AE-33 and the data were provided by Aerosol d.o.o., Ljubljana, Slovenia. The total concentration of BC is the result of traffic (BC_{tr}) and biomass burning (BC_{bb}) sources (Sandradewi et al., 2008). The Aethalometer was only installed at the end of November 2017, therefore BC data is not available for $W_{16–17}$.

Hourly observations of meteorological parameters including atmospheric pressure (hPa), global solar radiation (W m^{-2}), air temperature (°C), wind speed (m s^{-1}), wind direction (°), precipitation (mm h^{-1}) were provided by ARSO.

In addition to the measurements outlined above, total cloud cover (%) was obtained from the global data assimilation system (GDAS) model of NOAA/ARL (National Oceanic and Atmospheric Administration/Air Resources Laboratory).

2.3. ^{222}Rn observations and stability analysis

Atmospheric radon measurements were conducted using an AlphaGUARD PQ2000 PRO (Bertin Instruments) operating in diffusion mode with a 1-h integration time (Kikaj et al., 2019a; Kikaj and Vaupotič, 2017). The instrument was mounted 1.5 m a.g.l., within a Stevenson Screen instrument shelter. The AlphaGUARD has a lower limit of detection (LLD) of 2 Bq m^{-3}. Setup in this way it is expected that > 95% of the measured radon represents the isotope ^{222}Rn (Kochowska et al., 2009). Therefore, relative to the AlphaGUARD's measurement uncertainty for typical outdoor ambient radon monitoring conditions, contributions of isotopes ^{220}Rn (thoron) and ^{219}Rn (actinon) to the overall radon signal can be ignored.

Radon-based classification of diurnal timescale changes in stability ($^{222}Rn_{DS}$) have already been described by S. Chambers et al., 2019b; S. D. Chambers et al., 2019a and Kikaj et al. (2019b). Briefly, the approach involves isolating mixing-related (diurnal) changes in near-surface radon concentrations by estimating and removing air mass fetch effects, and then assigning stability thresholds to mean values of radon accumulation within a defined nocturnal window (10h). Corresponding daytime mixing states for each 24-h period are inferred from nocturnal conditions based on an assumption of short-term atmospheric persistence. The number of stability classes that can be distinguished in a statistically robust manner (typically 3 to 5) depends on the size of the available dataset.

Radon-based identification of synoptic timescale changes in the ABL mixing state ($^{222}Rn_{SS}$) (specifically PTI events), was first described by Kikaj et al. (2019a). Briefly, this method involves separating synoptic timescale variability in radon concentration from contributions occurring at other timescales, and then comparing the magnitudes of radon variability occurring at diurnal and synoptic timescales. When synoptic contributions to radon variability exceed the typical magnitude of diurnal ones for more than two consecutive days, a PTI event is considered to have occurred.

A summary of the six mixing classes (5 diurnal and 1 synoptic) for measurements at the SAB site that resulted from our combination of the above two classification techniques ($^{222}Rn_{DS}$ and $^{222}Rn_{SS}$) is presented in Table 1. The table also provides a relative breakdown of the number of events in each mixing class experienced in each winter period. Class #6 (PTI) days of each winter have been further subdivided into "strong"

Table 1
Summary and description of the 24-h radon-based atmospheric mixing classes assigned to SAB measurements for $W_{16–17}$ (December 2016–February 2017) and $W_{17–18}$ (December 2017–February 2018). Occurrence frequency (as a % of each 90-day winter period) of each stability class for both winters is also provided.

24-h mixing class	$W_{16–17}$ (%)	$W_{17–18}$ (%)	Night-time stability conditions	Daytime stability conditions	Expected meteorological conditions
#1	12	7	Mixed fetch or non-stationary	Mixed fetch or non-stationary	Moderate to strong gusty winds, often cloudy associated with passing strong synoptic systems or fronts, precipitation is common.
#2	20	15	Near-neutral	Near-neutral	Moderate to strong winds, often overcast, precipitation is common.
#3	19	19	Weakly stable	Weakly unstable	Light to moderate winds, broken cloud or overcast, possible precipitation.
#4	15	15	Moderately stable	Moderately unstable	Light winds, scattered clouds, precipitation is uncommon.
#5	14	14	Most stable	Most unstable	Calm to light wind, mostly clear sky, typically no precipitation.
#6	20	30	Persistent temperature inversion	Persistent temperature inversion	Calm gradient wind, foggy or low-level clouds, no precipitation.

Table 2
Quantile ranges of the amplitude of diurnal radon variability during persistent temperature inversion (PTI) events for $W_{16–17}$ (December 2016–February 2017) and $W_{17–18}$ (December 2017–February 2018).

Quantile ranges	$W_{16–17}$ (Bq m^{-3})	$W_{17–18}$ (Bq m^{-3})
10th	2	1
50th	7	4
90th	13	9

and "weak" categories based on the amplitude of diurnal radon variability. The selection threshold in this case was chosen to be the median (50th percentile) amplitude of diurnal radon variability during PTI events (Table 2). PTI days under the 50th percentile value are consider to be weak PTI events, and days that exceeded the 50th percentile value are consider to be strong PTI events.

3. Results and discussion

3.1. Meteorological characteristics of radon-based mixing classes

Two of the strongest meteorological indicators of the atmospheric mixing state are wind speed and the near-surface vertical temperature gradient. In the absence of vertical temperature gradient measurements at this site we found that the time rate of change in 2 m air temperature provided a better contrast between atmospheric mixing states than the observed hourly 2 m temperature record.

Class #1 days were characterized by strong and highly variable nocturnal wind speeds (Fig. 2a), consistent with non-stationary synoptic conditions (e.g. frontal passages), as described by Podstawczyńska and Chambers (2018). The non-stationary nature of these days violates important assumptions of the $^{222}Rn_{DS}$ method (Chambers et al., 2019b) and, as a result, complicates the interpretation of urban air quality statistics. Therefore, class #1 events (constituting only 7–12% of observations; Table 1) will be excluded from further discussion in this paper. Class #2 days had the highest nocturnal mean wind speeds (1.5–2 m s^{-1}), whereas the corresponding wind speed for class #5 days was much lower (0.2–0.5 m s^{-1}). The lowest of all nocturnal mean wind speeds were recorded on strong PTI days (consistently ~0.2 m s^{-1}). The wind directions under stable and PTI conditions were consistent with drainage flow (NE) into the basin along the Sava River valley (Kikaj et al., 2019b).

The windy (near-neutral) class #2 days were characterized by the lowest diurnal amplitudes of 2 m air temperature, as evidenced by average time rates of change in temperature of ≤0.2 °C h^{-1} over the diurnal cycle (Fig. 2b). By contrast, on class #5 days average 2 m temperature changes of ~1.5 °C h^{-1} were observed around sunset and sunrise. The highest rates of temperature change (≥2 °C h^{-1}) were observed on strong PTI days. It is of interest to note that nocturnal mean wind speeds of class #4 and #5 days are higher for $W_{16–17}$ than $W_{17–18}$. However, the thermodynamic stability on $W_{16–17}$ nights is stronger, which acts to suppress vertical mixing. This is a good example of the combined influences of these two parameters on the net effects of nocturnal near-surface mixing processes, and the consistency of the results is testimony to the ability of radon observations, alone, to distinguish between these mixing conditions.

Generally, from class #2 to #5 days the intensity of daytime solar radiation increased (Fig. 2c), indicating a reduction in average cloud cover (see also Table 3). It is the reduction in cloud cover, particularly at night, that enables the increased rates of surface cooling/heating after sunset and sunrise exhibited in Fig. 2b. PTI events are known to occur under persistent cold-season anticyclonic conditions (see also Table 3). Usually the anticyclonic regime persists for several days, leading to the development of synoptic subsidence inversion layer (or basin "capping inversion"). The height of this layer is usually coincides with the average elevation of the summits surrounding the basin (Whiteman, 1982; Largeron and Staquet, 2016), and persists for the whole anticyclonic period. The fact that strong PTI events of both winter periods (as selected only by radon) exhibit more intense solar radiation than the weak PTI events, indicates that strong PTI events occur closer to the centre of the anticyclonic systems, where regional scale subsidence is strongest and the air driest; a hypothesis that is supported by the atmospheric pressure observations in Table 3. On the other hand, lower intensity of solar radiation on weak PTI events indicate the low-level cloud cover or/and fog occurrence (VanReken et al., 2017). The snow cover in $W_{17–18}$ was the reason that PTI events of this winter lasted longer than those of $W_{16–17}$ (Tables 1, 20% in $W_{16–17}$ and 30% in $W_{17–18}$). Snow-covered ground is cold across the whole diurnal cycle, and its white colour reflects almost all incoming solar radiation. Combined with shorter winter day lengths, this is one of the main mechanisms leading to the development and long durations of these inversion conditions (Whiteman et al., 2004).

The final piece of evidence regarding the efficacy of the radon-based scheme to objectively and effectively separate atmospheric conditions on diurnal and synoptic timescales is in the progressive reduction in daily mean precipitation observed from class #2 to class #6 days (Fig. 2d). These observations are consistent with the cloud cover and atmospheric pressure summary of Table 3, and give credence to the 'expected meteorological conditions' summarized in Table 1.

3.2. Diurnal variability of radon concentrations within each mixing class

Diurnal radon concentrations corresponding to each of the six radon-based atmospheric mixing classes for the two winter seasons ($W_{16–17}$ and $W_{17–18}$) are shown in Fig. 3a. The lowest amplitude of diurnal radon concentrations was observed on the windy class #2 days for both winters. Since radon concentrations serve as a good proxy for the behavior of local primary pollutants with surface-based sources, this is an indication that little diurnal accumulation of urban pollution would be expected at this site for nocturnal wind speeds ≥1.5 m s^{-1}. A similar conclusion was drawn by Sesana et al. (2003, 2006). The amplitude of the diurnal radon cycle (via nocturnal accumulation)

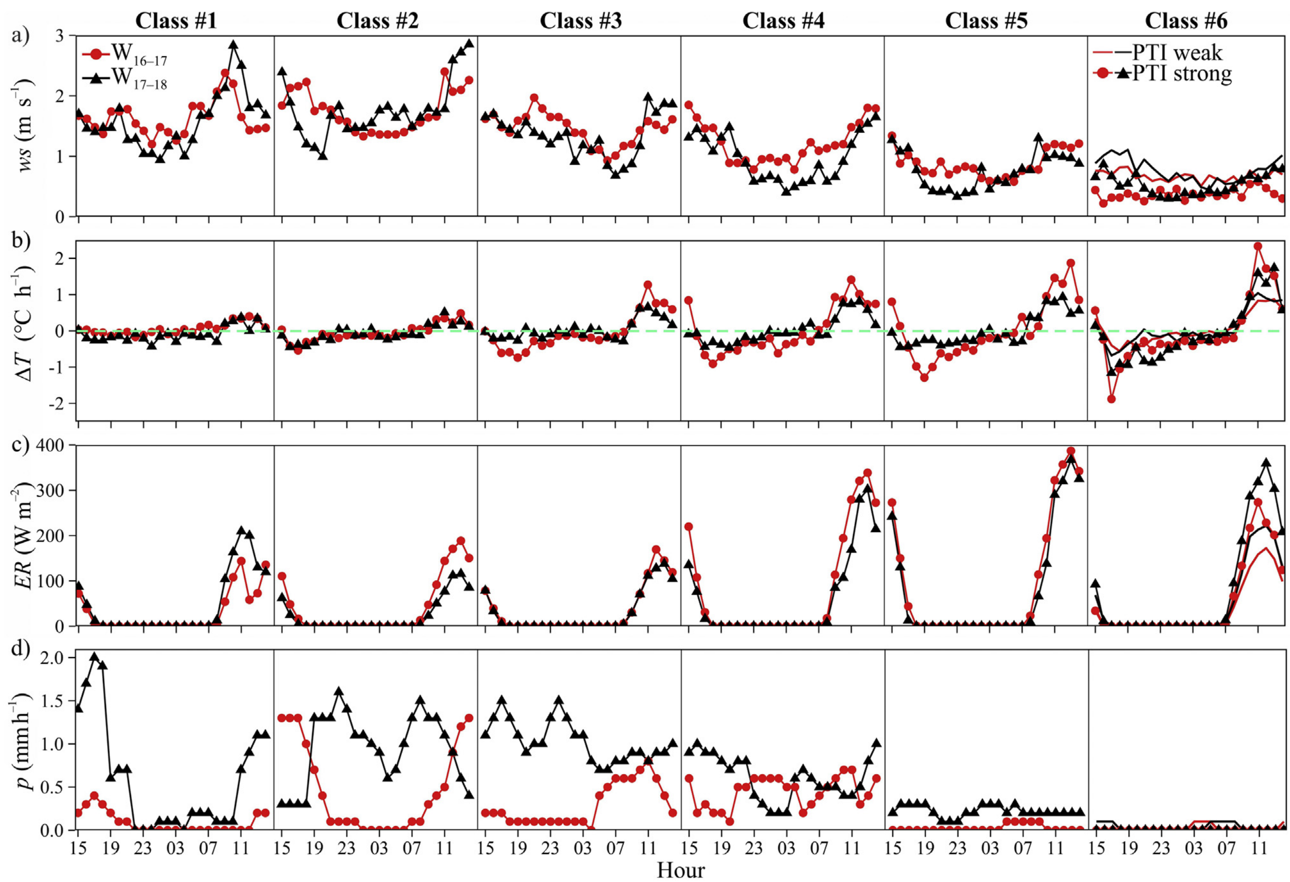

Fig. 2. Diurnal composite plots of hourly mean a) wind speed, b) time rate changes of air temperature, c) solar radiation, and d) precipitation for $W_{16–17}$ (December 2016–February 2017) and $W_{17–18}$ (December 2017–February 2018) and six radon-based atmospheric mixing classes.

Table 3
Daily mean atmospheric pressure and cloud cover (μ ± σ) for $W_{16–17}$ (December 2016–February 2017) and $W_{17–18}$ (December 2017–February 2018) and six radon-based atmospheric mixing classes.

24-h mixing class	$W_{16–17}$		$W_{17–18}$	
	P (hPa) μ ± σ	*CC* (%) μ ± σ	*P* (hPa) μ ± σ	*CC* (%) μ ± σ
#1	988 ± 11	51 ± 28	980 ± 5	76 ± 33
#2	985 ± 10	68 ± 35	979 ± 6	87 ± 18
#3	988 ± 8	55 ± 37	976 ± 9	87 ± 22
#4	989 ± 8	45 ± 36	978 ± 7	77 ± 26
#5	992 ± 8	33 ± 31	989 ± 7	44 ± 26
#6 (weak)	991 ± 6	55 ± 40	988 ± 7	57 ± 36
#6 (strong)	996 ± 6	16 ± 15	990 ± 6	33 ± 29

progressively increased from class #2 to class #5 conditions (Fig. 3a). In all mixing classes of $W_{16–17}$, the amplitude of the diurnal radon cycle was a factor of 2–3 higher than in $W_{17–18}$ (Fig. 2a). This was largely attributable to a slight reduction of radon exhalation rate (Levin et al., 2002; Mazur and Kozak, 2014) in $W_{17–18}$ due to the snow cover, higher ice content of the frozen soils and soil moisture. However, within each winter the radon source function was fairly consistent, enabling the increase of nocturnal radon concentrations from class #2 to #5 conditions to be interpreted as a decrease in mixing volume (formation of a progressively stronger and shallower stable nocturnal boundary layer, SNBL). This increase of radon concentration is consistent with the low wind speeds and increase thermodynamic stability of classes #4 and #5 as indicated in Fig. 2a and b.

Typically, the afternoons of classes #4 and #5 were characterized by low observed radon concentrations due to stronger convective mixing of the atmosphere (Fig. 3b). By contrast, during PTI events (class #6), the synoptic inversion layer and low wind speeds inhibit the vertical and horizontal dispersal of radon across the whole diurnal cycle, resulting in higher afternoon observed radon concentrations (Fig. 3b). Another contributing factor to the higher radon concentrations generally on PTI days is the extended air mass time over land resulting from the near-stagnant synoptic anticyclonic conditions.

As evident from Fig. 3a, the highest diurnal amplitude of local radon contribution was noted during strong PTI events, which cycle indicates the formation of a shallow (strong) SNBL within synoptic inversion layer around sunset that erodes after sunrise. The modest diurnal amplitude of local radon contribution of weak PTI events, on the other hand, indicated the presence of a deeper (weak) SNBL within the synoptic subsidence inversion layer.

3.3. Variability of pollutant concentration with atmospheric mixing class

The diurnal composites of air pollutants (BC_{tr}, NO_2, CO, BC_{bb}, PM_{10}, SO_2 and O_3) classified by the $^{222}Rn_{DS}$ and $^{222}Rn_{SS}$ for both winters, are shown in Fig. 4. The diurnal cycle of pollutants is mainly influenced by their source strengths and the diurnal and synoptic changes of atmospheric mixing. A clear distinction is evident between diurnal behavior of BC_{tr} (specifically related to vehicle emissions) on class #5 days and NO_2, CO, BC_{bb} and PM_{10} (related to either combustion, or a combination of traffic and combustion sources). Only BC_{tr} reflects a pronounced drop in source strength between 01:00–05:00 LT, when there are fewer vehicles on the roads, but some domestic heaters were still active. During classes #2 and #3 when diurnal variability of average temperature rate of change (Fig. 2b) was the lowest (overcast conditions) and the mean nocturnal wind speed was above 1 m s^{-1} (Fig. 2c) almost no accumulation of local (traffic related: BC_{tr}, NO_2, CO and domestic

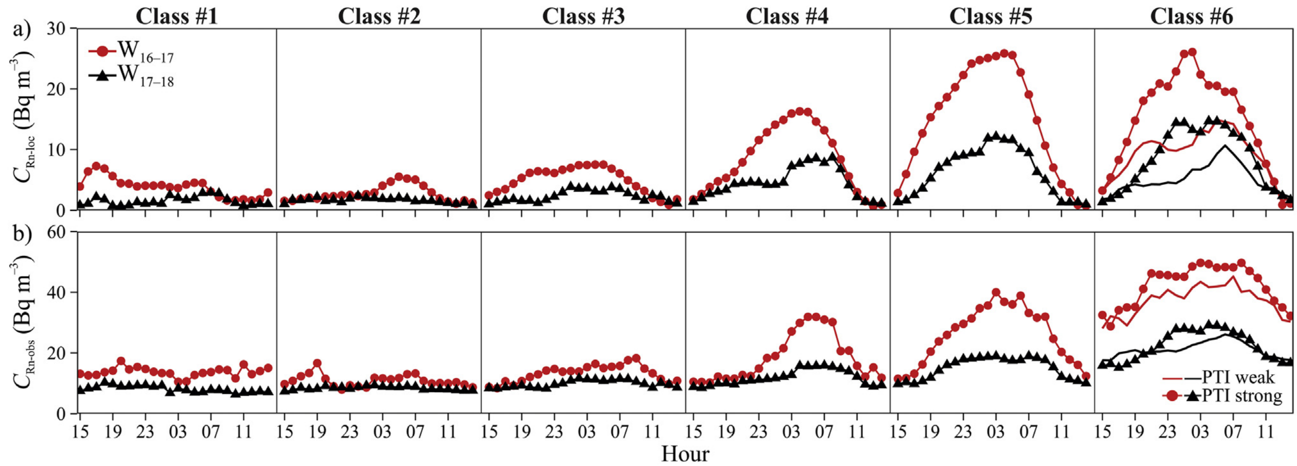

Fig. 3. Diurnal composite plots of hourly mean a) diurnal (local) radon contribution ($C_{\text{Rn-loc}}$), and b) observed radon concentration ($C_{\text{Rn-obs}}$) for $W_{16–17}$ (December 2016–February 2017) and $W_{17–18}$ (December 2017–February 2018) and six radon-based atmospheric mixing classes.

heating: CO, BC_{bb}, PM_{10}) pollution occurred (Fig. 4a–e). On class #4 and #5 days, the diurnal amplitude of locally-sourced pollutants increased (Fig. 4a–e), due to the near-calm wind conditions and strong thermal suppression (using average temperature rate of change as proxy) (Fig. 2c). Under such conditions (classes #4 and #5), BC_{tr} and NO_2 exhibited a bimodal diurnal distribution with one peak in morning (07:00–08:00 LT) and other in afternoon (17:00–19:00 LT) (Fig. 4a and b). These peaks are attributable to an overlap between "rush hour" vehicle emissions and a period of the day when the mixing depth is either low, or transitioning between day/night max/min values. On average, peak BC_{tr} and NO_2 concentrations on class #5 were a factor of 2–3 higher than for class #2 (Fig. 4a and b). The diurnal cycle of CO was more similar to those of combustion-dominated (BC_{bb} and PM_{10}) than traffic related pollutants. The pronounced diurnal peaks of CO, BC_{bb}, PM_{10} occurred between 21:00 LT and 23:00 LT (Fig. 4c–e), and concentrations remained high for few hours. During evening time, the traffic usually decreases, and residential heating increases as the air temperature drops.

Over the composites of classes #4 and #5, there were two periods when local pollutant concentrations reached minimum values: (i) in the morning (03:00–05:00 LT) when light katabatic drainage winds flush away some of the urban pollution, and (ii) in the afternoon (11:00–15:00 LT) when vertical mixing was the highest (deepest ABL) (Fig. 4a–e).

The amplitudes of diurnal cycles of traffic and domestic related pollutants on class #5 days were similar to those on class #6 days (PTI strong and weak). However, in an absolute sense a significant increase of pollutant concentrations was observed under PTI conditions due to the accumulation of pollutants either from upwind sources or under near-stagnant conditions, as evidenced by increased afternoon concentrations. The peak concentration of BC_{tr}, NO_2, CO, BC_{bb} and PM_{10} increased by a factor of 1.2–3 from most stable conditions (class #5) to PTI strong conditions (class #6) (Fig. 4a–e) as a consequence of an increase in source strength and decrease in SNBL under strong PTI conditions.

As evident from Fig. 4a–e, the diurnal cycle amplitudes of local pollutants (BC_{tr}, NO_2, CO, BC_{bb} and PM_{10}) under weak PTI conditions was lower than those observed under strong PTI conditions, when a stronger SNBL formed within the persistent synoptic subsidence inversion. For example, under strong PTI conditions, the diurnal PM_{10} amplitude was 52 μg m^{-3} (50–102 μg m^{-3}) in $W_{16–17}$ and 20 μg m^{-3} (31–51 μg m^{-3}) in $W_{17–18}$. By comparison, during corresponding weak PTI events, the diurnal PM_{10} amplitude decreased from 27 μg m^{-3} (61–88 μg m^{-3}) in $W_{16–17}$ to 11 μg m^{-3} (32–43 μg m^{-3}) in $W_{17–18}$. Although the concentrations typically trend downward from night to day, the daytime concentrations of pollutants under PTI conditions (weak and strong) did not reach the low daytime levels characteristic of class #5 conditions. The stagnant anticyclonic conditions inhibited the daytime mixing that usually disperses accumulated nocturnal pollution on class #5 days.

The key differences in local pollutant concentrations observed between the two winters were attributable to a combination of changes in stability and changes in source strength. In $W_{16–17}$ there was a larger traffic source near the monitoring site (Section 2.1), the domestic heating source was also larger (due to lower air temperatures), and the lack of snow cover lead to increased nocturnal atmospheric stability. Combined, these factors lead to higher pollutant concentrations under class #5 and PTI conditions in $W_{16–17}$ compared with $W_{17–18}$.

Within all mixing classes the diurnal cycles of SO_2 and O_3 were markedly different compared with those of locally-generated primary pollutants (Fig. 4f–g). In the case of SO_2, peak concentrations occurred after the breakdown of the nocturnal inversion, when the ABL was deeper and more well-mixed. By contrast, SO_2 concentrations reduced at night when the SNBL isolates the near-surface observations from more remote influences. Consequently, while local traffic and domestic heating are expected to contribute a little to SO_2 concentrations in Ljubljana, remote SO_2 sources dominated in the winters of this study. As an example, SO_2 concentrations were higher over the whole diurnal cycle under weak PTI conditions in $W_{16–17}$ when wind speeds were slightly higher, than for the strong PTI conditions.

Compared with radon and locally-sourced pollutants, the atmospheric mixing state appeared to have the opposite effect on O_3 concentrations. This is largely due to the fact that O_3 is a highly reactive, photochemically-produced secondary pollutant. When trapped in a shallow inversion layer (e.g. classes #4, #5 and #6) O_3 either reacts with surface roughness elements (dry deposition), or gets titrated by NO emissions. Comparing night-time O_3 levels on strong and weak PTI events, the lowest values were found on strong PTI events due to the stronger SNBL formation, which traps NO. By comparison, on class #2 and #3 nights, with the increase of wind speeds, the highest nocturnal O_3 concentrations were found due to remotely-sourced O_3 being mixed down to the surface from the residual layer or troposphere (Querol et al., 2018). As nocturnal wind speeds decrease from class #3 to #4 conditions, a decrease of O_3 levels in the morning is noticed due to the titration by NO in the morning peak hour traffic. The highest overall O_3 concentrations were observed during the day under class #5 conditions, when skies were clear and solar radiation was most intense.

The combined radon-based atmospheric stability techniques performed in this study helps to separate "uncontrollable" (natural) influences from controllable influences on pollution variability.

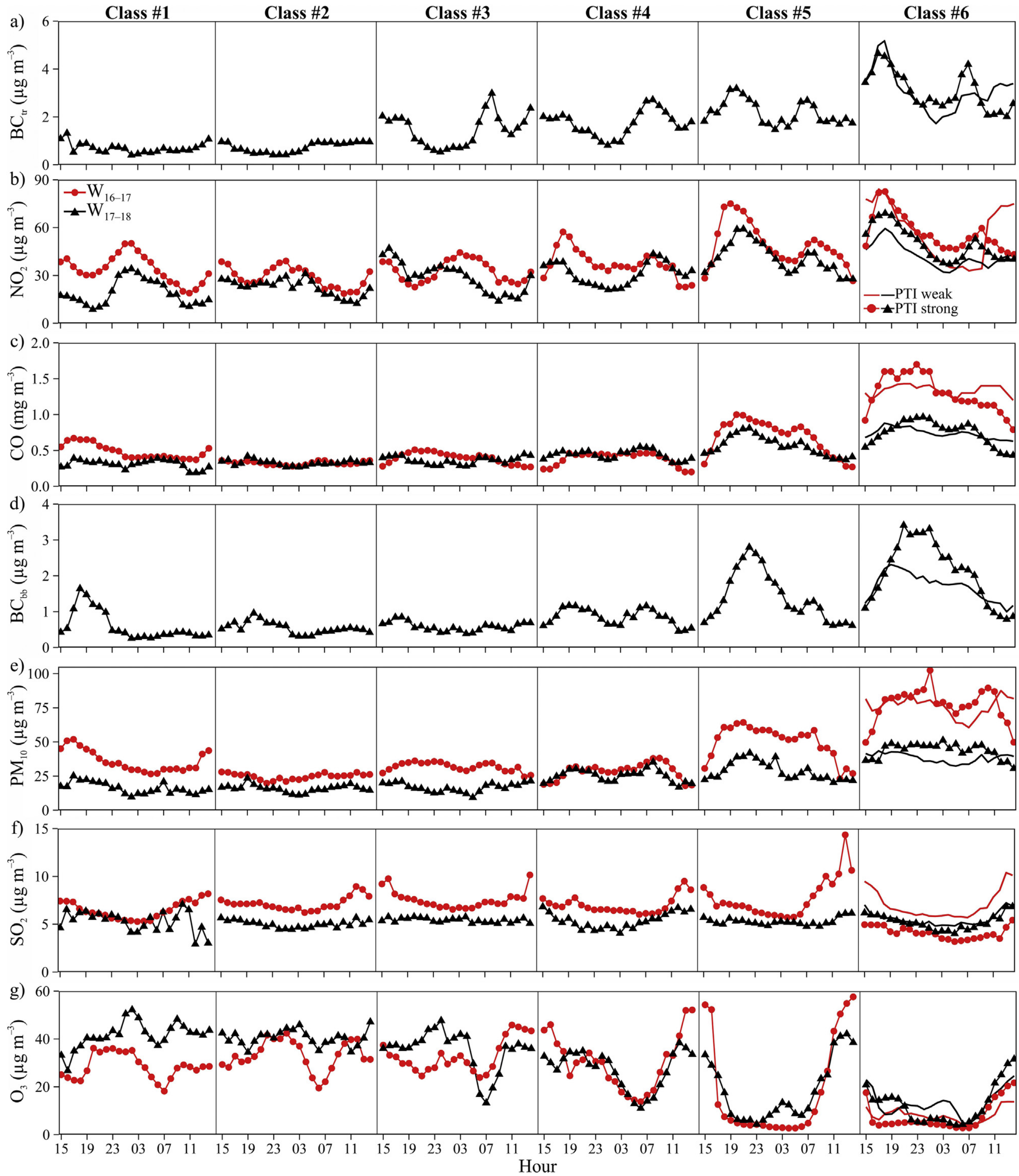

Fig. 4. Diurnal composite plots of hourly mean: a) BC$_{tr}$, b) NO_2, c) CO, d) BC$_{bb}$, e) PM_{10}, f) SO_2 and g) O_3 for W$_{16–17}$ (December 2016–February 2017) and W$_{17–18}$ (December 2017–February 2018) and six radon-based atmospheric mixing classes.

Consequently, the results summarized in Figs. 2, 3 and 4 also constitute a valuable benchmarking dataset that could be used in future evaluation studies of chemical transport model performance (e.g. Chambers et al., 2019b). Repeating this study in the future and comparing diurnal pollutant variability under well-constrained class #5 and PTI conditions would also provide valuable information regarding the efficacy of any imposed pollution mitigation measures.

3.4. *Cross boundary pollution transport*

In order to better distinguish distant pollution sources (e.g. industry, electricity production) from local Ljubljana emissions we investigated SO_2 and O_3 concentrations under only the more windy conditions (classes #1 to #3). Here we also considered class #1 days since strong frontal weather systems are also effective at transporting pollution. As an example of the contrasting airmass fetch characteristics between moderate-to-strong gradient wind conditions (classes #1 and #2) and

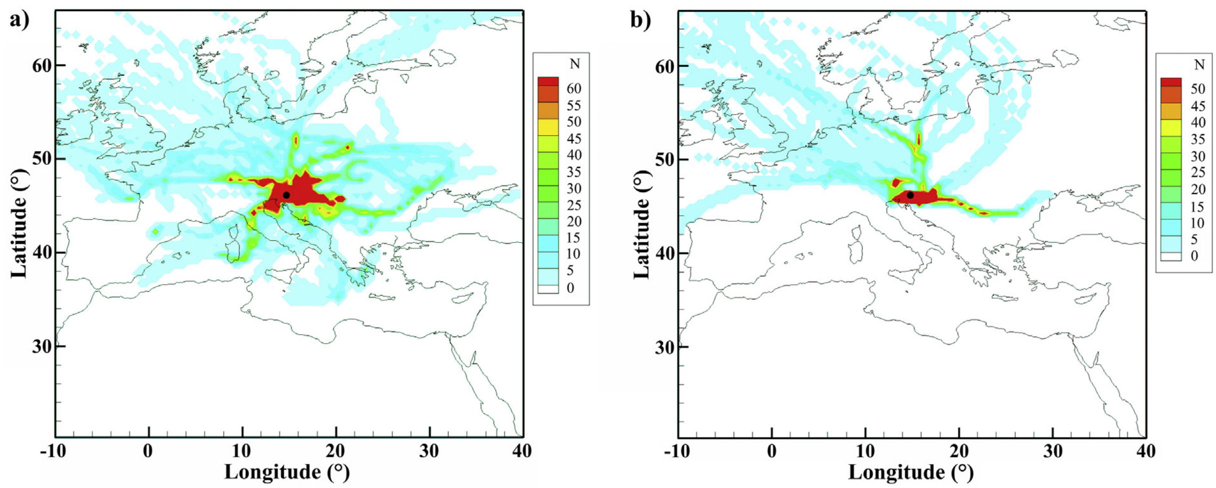

Fig. 5. Trajectory density plots of a) radon-based atmospheric mixing classes #1 and #2, and b) radon-based atmospheric mixing class #5 for W_{16-17} (December 2016–February 2017) and W_{17-18} (December 2017–February 2018). *N* represents the number of times a trajectory passes through a 0.5 × 0.5 grid cell. Ljubljana sub-Alpine Basin is indicated with a black circle.

weak gradient wind conditions (class #5), Fig. 5 compares density plots constructed from 4-day NOAA HYSPLIT v4.0 back trajectories with a starting height of 100 m a.g.l. Shading in these figures represents the different number of times that individual trajectories pass through a given grid cell. Based on the red through green shading on these plots, it is evident that the strong gradient wind conditions represent fetch regions in all directions surrounding Ljubljana, over a large portion of Europe (Fig. 5a). By contrast, airmass fetch for mixing class #5 days (with weak gradient winds), represents a much smaller area, predominantly to the east of Ljubljana, and completely excludes the Po Valley region (Fig. 5b). To minimise the chance of large local contributions to this signal we also employed a "diurnal sampling window" (between 11:00–15:00 LT), to best capture times when the near-surface pollutant observations were the most representative of the whole ABL. According to the GDAS mixing height information, this diurnal window represents the time of deepest, least variable mixing depth that would be representative of the largest fetch region. Further, to better identify the likely specific sources of remotely-generated pollution, we used the Conditional Probability Function technique (CPF) (Uria-Tellaetxe and Carslaw, 2014), which estimates the probability of pollutant concentrations (> 90th percentile) occurring as a function of wind direction. CPF plots of SO_2 and O_3 for the three $^{222}Rn_{DS}$ classes (#1, #2 and #3) of W_{16-17} and W_{17-18} based on data within the 11:00–15:00 LT sampling window are shown in Figs. 6 and 7.

On class #1, #2 and #3 days, the O_3 and SO_2 concentrations generally began to increase from background values as wind speeds increased beyond 2–3 m s^{-1} (Figs. 6 and 7). These results suggested that O_3 and SO_2 concentrations were dominated by remote sources under these conditions, since we have shown that little diurnal accumulation of local emissions is observed for wind speeds ≥1.5 m s^{-1}. Hourly SO_2 (> 90th percentile) ranged 12–32 μg m^{-3} (6.7–10.0 μg m^{-3}) in W_{16-17} (W_{17-18}) (Figs. 6 and 7). While hourly O_3 concentrations (> 90th percentile) ranged 72–95 μg m^{-3} (65–100 μg m^{-3}) in W_{16-17} (W_{17-18}) (Figs. 6 and 7). As evident from Figs. 6 and 7, in case of O_3, the highest probability (0.9–1.0) was found when the directions were SW (Po Valley/Port of Koper) or NE (Zasavje area). Probabilities were less consistent (0.6) in the easterly direction. The CPF plots clearly reveal four potential sources for SO_2 (NE-Zasavje/Šoštanj area, E-Toplarna power plant, and SW-Po Valley, shipping emissions-Port of Koper) with probability range from 0.04 to 1 (Figs. 6 and 7). Taking into consideration a conversion rate of 0.02 h^{-1} for $SO_2 \rightarrow SO_4^{2-}$ oxidation during the long-range transport (Seinfeld and Pandis, 2006), and assuming that pure SO_2 was emitted at the identified source regions, then SO_4^{2-}/ SO_2 ratio would have become 0.6, 1.6, and 3.3 after 24 h, 48 h and 72 h of transport, respectively (typical transport times from Po Valley to Ljubljana indicated by HYSPLIT back trajectories under near-neutral conditions). Thus, SO_2 concentration becomes 61%, 38% and 23% of initial SO_2 after the 24 h, 48 h and 72 h of transport, respectively.

In addition to the prevailing meteorology, the ability to detect sources at specific receptor locations also depends on the terrain surrounding the observation site. Terrain influences for the SAB site are expected to influence that SW/SSW wind to be channeled up to the basin, therefore, the bivariate polar plot reveals exactly the identified pollution sources. The same, when winds approach from the NE/E directions, the dispersion of pollutants is almost in straight lines unaffected by hills going through the Sava Basin.

3.5. Health implications

Based on mean air quality data from Fig. 4, the worst potential public exposure in Ljubljana urban background site occurs during the most stable (nights of class #5) and strong PTI (class #6) conditions. Class #5 conditions comprise 14% and PTI conditions 20–30% of observations for winter season. Due to that we indicated the variability (μ ± 1σ) in air quality associated only with these two classes (Fig. 8). The μ ± 1σ PM_{10} concentrations exceeded both EU and WHO values during the class #5 and strong PTI events (Fig. 8 and Table 4). The μ ± 1σ concentrations of CO, NO_2, SO_2 and O_3 were well below hourly and daily maximum of EU and WHO guidelines values. By looking into the μ ± 2σ, which is a good indication of the absolute hourly peak values clearly NO_2 also sometimes exceeded both EU and WHO values during the class #5 and strong PTI events (Fig. 8 and Table 4). Due to their high number concentrations and small diameters BC have higher surface area per mass to absorb toxic materials than larger particles (Sun et al., 2019), however their concentration is not yet regulated by either EU or WHO. Peak BC_{tr} (BC_{bb}) concentrations during strong PTI events were 5 ± 16 μg m^{-3} (3 ± 5 μg m^{-3}). In an investigation of health effects of black carbon particles, Jannsen et al. (2011) concluded that daily mortality or hospital admissions were generally higher for increases in black carbon than for PM_{10} and $PM_{2.5}$.

4. Conclusions

The main aim of this study was to combine, for the first time, diurnal ($^{222}Rn_{DS}$) and synoptic ($^{222}Rn_{SS}$) timescale radon-based

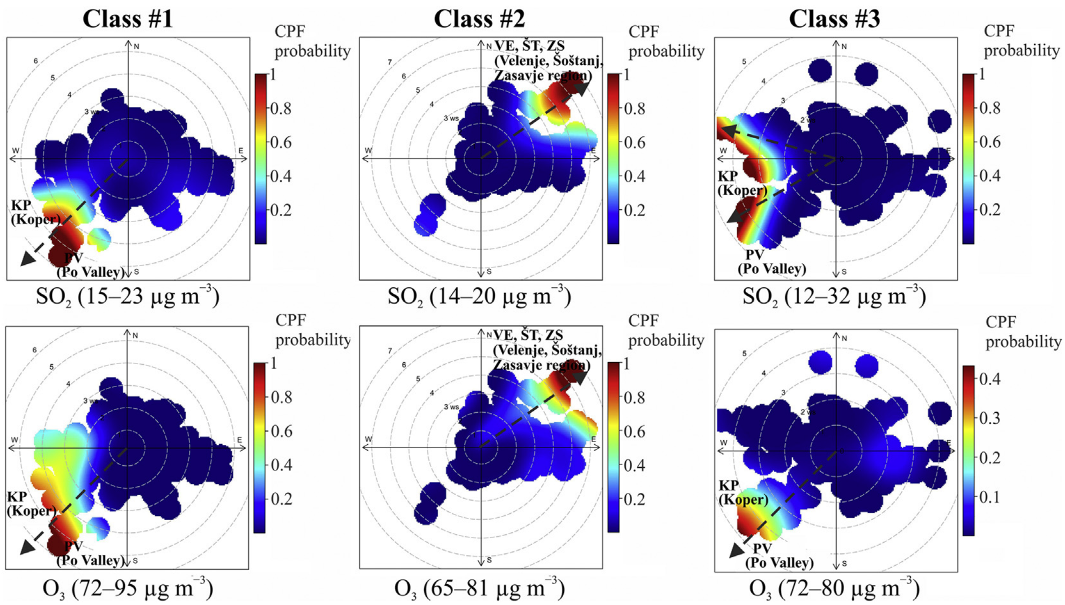

Fig. 6. The Conditional Probability Function (CPF) plots of SO_2 and O_3 for concentrations > 90th percentile during "diurnal sampling window" (11:00–15:00 LT) of for $W_{16–17}$ (December 2016–February 2017) for radon-based atmospheric mixing classes #1, #2 and #3. The dashed lines show the direction of potential known sources (see text for details).

atmospheric stability classification methods to improve understanding of urban pollution variability in the urban sub-Alpine site Ljubljana. For this purpose, hourly air quality, meteorology and atmospheric radon concentration were monitored during two winter periods of 2016–2017 ($W_{16–17}$) and 2017–2018 ($W_{17–18}$). The combination of the two methods ($^{222}Rn_{DS}$ and $^{222}Rn_{SS}$), resulted in 5 diurnal and 1 synoptic (persistent temperature inversion, PTI) mixing classes being defined. Furthermore, "strong" and "weak" categories of the PTI class were defined based on diurnal radon variability within that class.

Key differences in urban pollutant concentrations observed between the two winters were attributable to a combination of changes in stability and changes in source strengths. In $W_{16–17}$ there was a 28% larger traffic source near the monitoring site and the domestic heating source was also 17% larger (due to lower air temperatures). Based on the meteorological conditions for the 6 distinct mixing states, the thermodynamic stability on stable nights of $W_{16–17}$ was stronger, which acts to suppress vertical mixing. Combined, these factors lead to higher pollutant concentrations under stable (class #5) and PTI conditions in $W_{16–17}$ compared with $W_{17–18}$. Under the more windy conditions for both winters results suggested that SO_2 concentrations were dominated by remote sources (primarily from the Po Valley region). The diurnal characteristics of O_3 concentrations indicated both local and remote sources. Little diurnal accumulation of local pollutants (BC_{tr}, NO_2, CO, BC_{bb} and PM_{10}) was observed for wind speeds ≥ 1.5 m s^{-1}.

The combined radon-based atmospheric classification methods performed in this study help to separate "uncontrollable" (meteorology, geographic setting, topographic effects, and cross-boundary pollution) influences from controllable (source strength) influences on pollution

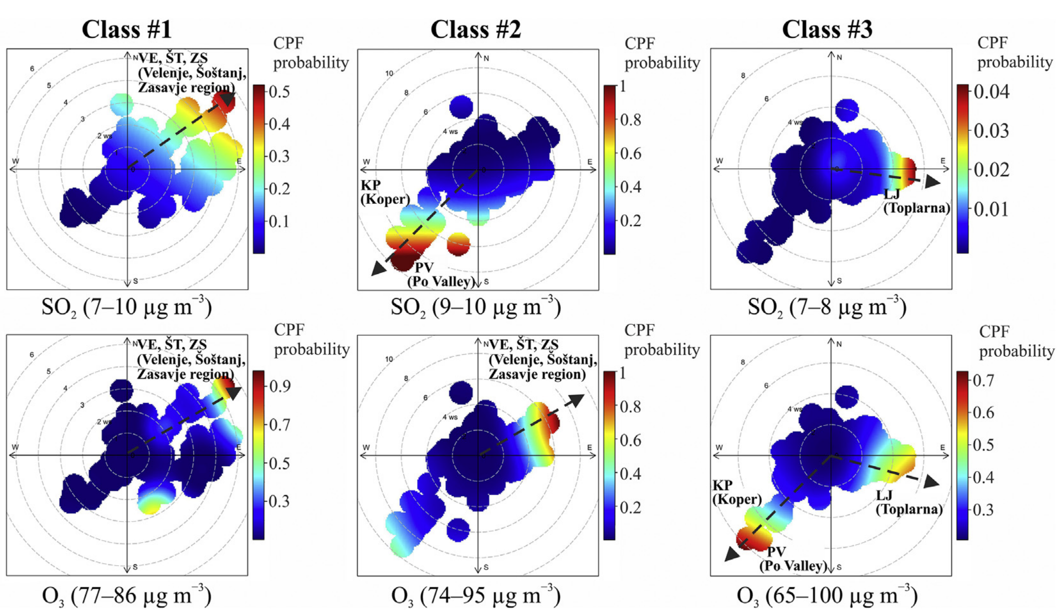

Fig. 7. The Conditional Probability Function (CPF) plots of SO_2 and O_3 for concentrations > 90th percentile during "diurnal sampling window" (11:00–15:00 LT) of for $W_{17–18}$ (December 2017–February 2018) for radon-based atmospheric mixing classes #1, #2 and #3. The dashed lines show the direction of potential known sources (see text for details).

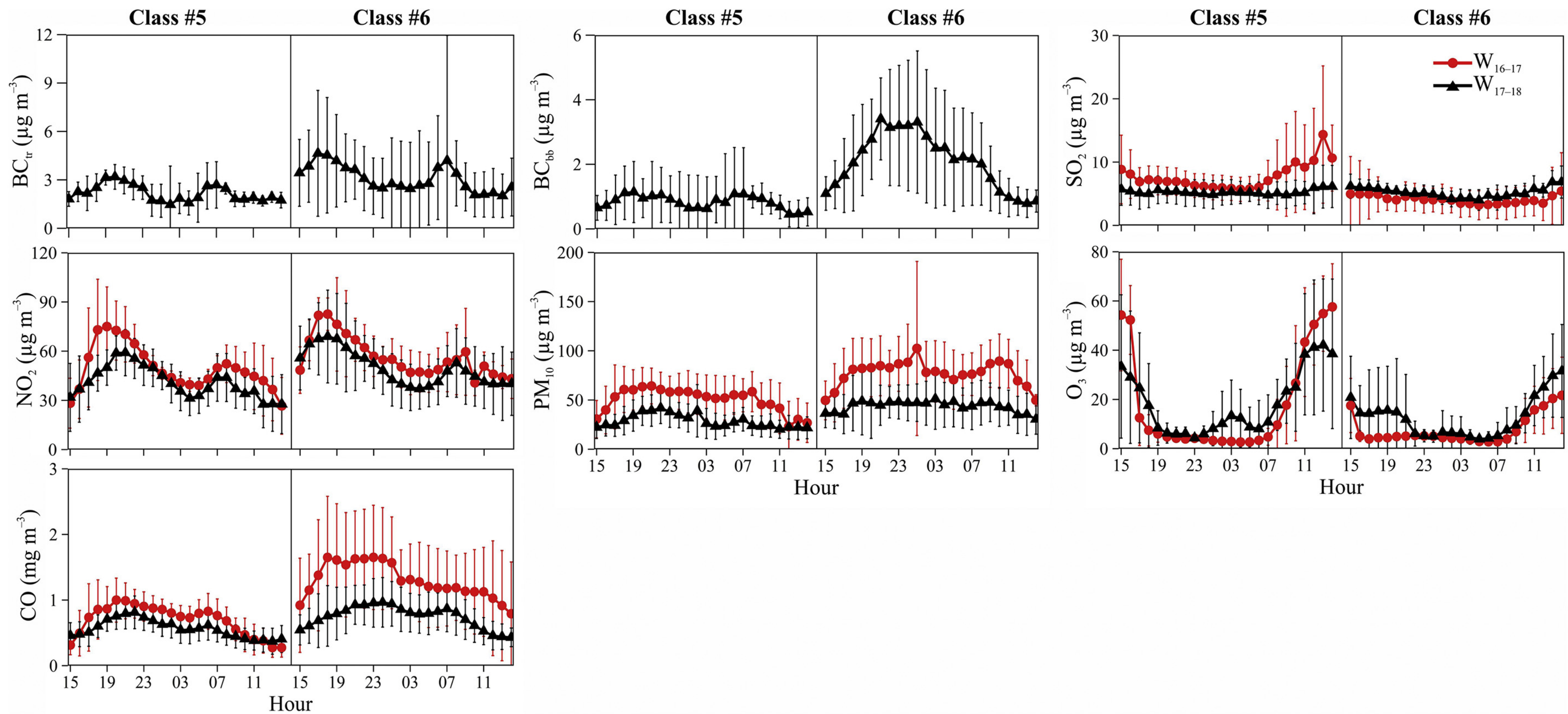

Fig. 8. Comparison of variability associated with the highest pollution (BC_{tr}, NO_2, CO, BC_{bb}, PM_{10}, SO_2 and O_3) concentration events during class #5 and class #6 (strong PTI) mixing conditions for W_{16-17} (December 2016–February 2017) and W_{17-18} (December 2017–February 2018). Whiskers represent ± σ.

Table 4
Air quality standards for the protection of health, given by the European Union (EU) and World Health Organization (WHO). Air quality standards in brackets represent those stipulated by the WHO (EEA, 2018).

	CO mg m^{-3}	NO_2 µg m^{-3}	PM_{10} µg m^{-3}	SO_2 µg m^{-3}	O_3 µg m^{-3}
Max daily			50 (50)	125 (20)	
Max daily 8-h mean	10 (10)				120 (100)
Max hourly	(30)	200		350	240 (200)

variability. Consequently, the results also constitute a valuable benchmarking dataset that could be used in future evaluation studies of chemical transport model performance. Repeating this study in the future and comparing diurnal pollutant variability under well-constrained most stable and PTI conditions would also provide valuable information regarding the efficacy of any imposed pollution mitigation measures. Based on the success of this winter study, the next step is to characterize diurnal and synoptic timescale influences on the atmospheric mixing state at this site year-round, and use this information in conjunction with detailed traffic density data to better relate specific source strengths to observed air quality variability in Ljubljana.

Author contribution statement

The investigation was jointly conceptualized by DK, SC, MK and JV. Radon monitoring instrumentation was deployed and managed by DK and JV, and black carbon data by MK. Data collection and curation was performed by DK. Formal data analysis was performed by DK. Acquisition of funding for the research was arranged by JV. The research methodology was jointly developed by DK and SC and investigation jointly conducted by DK and JV. The project was administered by JV, with JV and SC responsible for supervision. All visualization of data, concepts, and results was performed by DK, while the script written to acquire, separate and process the back trajectories for visualization was performed by JC. DK wrote the complete original draft of the paper, which was subsequently edited and reviewed jointly by DK, SC, MK, JC and JV.

Declaration of Competing Interest

The authors declare that they have no known competing financial interests or personal relationships that could have appeared to influence the work reported in this paper.

Acknowledgements

The authors acknowledge the financial support from the Slovenian Research Agency (research core funding No. P1-0143 and research project STRAP – Sources, TRAnsport and fate of persistent air Pollutants in the environment of Slovenia No. J1-1716) and from the Public Scholarship, Development, Disability and Maintenance Fund of the Republic of Slovenia (contract No. 11011-44/2016-18). The authors also gratefully acknowledge the Slovenian Environmental Agency for the permission provided and the assistance by installing the weather instrument shelter for radon monitoring on their land and for providing the meteorological and air quality data.

References

Allegrini, I., Febo, A., Pasini, A., Schiarini, S., 1994. Monitoring of the nocturnal mixed layer by means of particulate radon progeny measurement. J. Geophys. Res. 99, 18765–18777.

ARSO, Slovenian Environment Agency (Slovenian): Agencija Republike Slovenije za Okolje), 2017. Climate characteristics of Ljubljana - Wind Rose for the City of Ljubljana.

Ayers, G.P., Bigg, E.K., Turvey, D.E., Manton, M.J., 1982. Urban influence on condensation nuclei over a continent. Atmos. Environ. 16, 951–954.

Baasandorj, M., Hoch, S.W., Bares, R., Lin, J.C., Brown, S.S., Millet, D.B., Martin, R., Kelly, K., Zarzana, K.J., Whiteman, C.D., Dube, W.P., Tonnesen, G., Jaramillo, I.C., Sohl, J., 2017. Coupling between chemical and meteorological processes under persistent cold-air pool conditions: evolution of wintertime $PM_{2.5}$ pollution events and N_2O_5 observations in Utah's Salt Lake Valley. Environ. Sci. Technol. 51, 5941–5950. https://doi.org/10.1021/acs.est.6b06603.

Bigi, A., Bianchi, F., De Gennaro, G., Di Gilio, A., Fermo, P., Ghermandi, G., Prévôt, A.S.H., Urbani, M., Valli, G., Vecchi, R., Piazzalunga, A., 2017. Hourly composition of gas and particle phase pollutants at a central urban background site in Milan, Italy. Atmos. Res. 186, 83–94.

Bowen, B., 1994. Long-term tracer at Los Alamos, New Mexico. Part II: Evalution and comparison of several methods to determine dispersion coefficients. J. Appl. Meteorol. 33, 1236–1254.

Chambers, S., Williams, A.G., Zahorowski, W., Griffiths, A., Crawford, J., 2011. Separating remote fetch and local mixing influences on vertical radon measurements in the lower atmosphere. Tellus Ser. B Chem. Phys. Meteorol. 63, 843–859. https://doi.org/10.1111/j.1600-0889.2011.00565.x.

Chambers, S.D., Podstawczyńska, A., Pawlak, W., Fortuniak, K., Williams, A., Griffiths, A., 2019a. Characterising the state of the urban surface layer using Radon-222. J. Geophys. Res. Atmos. 124, 770–788.

Chambers, S.D., Williams, A.G., Crawford, J., Griffiths, A.D., 2015. On the use of radon for quantifying the effects of atmospheric stability on urban emissions. Atmos. Chem. Phys. 15, 1175–1190. https://doi.org/10.5194/acp-15-1175-2015.

Chambers, S.D., Galeriu, D., Williams, A.G., Melintescu, A., Griffiths, A.D., Crawford, J., Dyer, L., Duma, M., Zorila, B., 2016a. Atmospheric stability effects on potential radiological releases at a nuclear research facility in Romania: Characterising the atmospheric mixing state. J. Environ. Radioact. 154, 68–82. https://doi.org/10.1016/j.jenvrad.2016.01.010.

Chambers, S., Guérette, E.-A., Monk, K., Griffiths, A., Zhang, Y., Duc, H., Cope, M., Emmerson, K., Chang, L., Silver, J., Utembe, S., Crawford, J., Williams, A., Keywood, M., 2019b. Skill-testing chemical transport models across contrasting atmospheric mixing states using Radon-222. Atmosphere 10, 25. https://doi.org/10.3390/atmos10010025.

Chambers, S.D., Kang, C.-H., Williams, A.G., Crawford, J., Griffiths, A.D., Kim, K.-H., Kim, W.-H., 2016b. Improving the representation of cross-boundary transport of anthropogenic pollution in East Asia using Radon-222. Aerosol Air Qual. Res. 16, 958–976. https://doi.org/10.4209/aaqr.2015.08.0522.

Chambers, S.D., Kim, K.H., Kwon, E.E., Brown, R.J.C., Griffiths, A.D., Crawford, J., 2017. Statistical analysis of Seoul air quality to assess the efficacy of emission abatement strategies since 1987. Sci. Total Environ. 580, 105–116. https://doi.org/10.1016/j.scitotenv.2016.09.151.

Cohen, L.D., Barr, S., Krablin, R., Newstein, H., 1972. Steady-state vertical turbulent diffusion of radon. J. Geophys. Res. 77, 2654–2668.

Crawford, J., Chambers, S., Cohen, D., Williams, A., Griffiths, A., Stelcer, E., 2016. Assessing the impact of atmospheric stability on locally and remotely sourced aerosols at Richmond, Australia, using Radon-222. Atmos. Environ. 127, 107–117. https://doi.org/10.1016/j.atmosenv.2015.12.034.

Dons, E., Int Panis, L., Van Poppel, M., Theunis, J., Wets, G., 2012. Personal exposure to black carbon in transport microenvironments. Atmos. Environ. 55, 392–398. https://doi.org/10.1016/j.atmosenv.2012.03.020.

EEA: Air quality in Europe, 2016. 2016 Report.

EEA: Air quality in Europe, 2017. 2017 Report.

EEA: Air quality in Europe, 2018. 2018 Report.

Fiorella, R.P., Bares, R., Lin, J.C., Ehleringer, J.R., Bowen, G.J., 2018. Detection and variability of combustion-derived vapor in an urban basin. Atmos. Chem. Phys. 18, 8529–8547. https://doi.org/10.5194/acp-18-8529-2018.

Gjerek, M., Koleša, T., Logar, M., Matavž, L., Murovec, M., Paradiž, B., Rus, M., Žabkar, R., 2016. Kakovost zraka v Sloveniji v letu 2016. Tech. Rep. ARSO.

Gjerek, M., Koleša, T., Logar, M., Matavž, L., Murovec, M., Paradiž, B., Rus, M., Žabkar, R., 2017. Kakovost zraka v Sloveniji v letu 2017. Tech. Rep. ARSO.

Goudie, A.S., 2014. Desert dust and human health disorders. Environ. Int. 63, 101–113. https://doi.org/10.1016/j.envint.2013.10.011.

He, T., Chen, Y., Staničč, S., Bergant, K., Gao, F., Hua, D., 2018. Properties of tropospheric aerosols observed over Southwest Slovenia. J. Quant. Spectrosc. Radiat. Transf. 217, 380–387. https://doi.org/10.1016/j.jqsrt.2018.06.009.

Hitzenberger, R., Ctyroky, P., Berner, A., Turšič, J., Podkrajšek, B., Grgić, I., 2006. Size distribution of black (BC) and total carbon (TC) in Vienna and Ljubljana. Chemosphere 65, 2106–2113. https://doi.org/10.1016/j.chemosphere.2006.06.042.

Janssen, N.A.H., Hoek, G., Simic-lawson, M., Fischer, P., Van Bree, L., Brink, H., Keuken, M., Atkinson, R.W., Anderson, H.R., Brunekreef, B., Cassee, F.R., 2011. Black carbon and health effects of airborne particles compared with PM_{10} and $PM_{2.5}$. Environ. Health Perspect. 119, 1691–1699. https://doi.org/10.1289/ehp.1003369.

Kahl, J.D.W., Chapman, H.L., 2018. Atmospheric stability characterization using the Pasquill method: a critical evaluation. Atmos. Environ. 187, 196–209. https://doi.org/10.1016/j.atmosenv.2018.05.058.

Kallos, G., Astitha, M., Katsafados, P., Chris, S., 2006. Long-range transport of anthropogenically and naturally produced particulate matter in the Mediterranean and North Atlantic: current state of knowledge. J. Appl. Meteorol. Climatol. 46, 1230–1251. https://doi.org/10.1175/JAM2530.1.

Karanasiou, A., Mihalopoulos, N., 2013. Air Quality in Urban Environments in the Eastern Mediterranean. In: Viana, M. (Ed.), Urban Air Quality in Europe. Springer, pp. 219–238.

Kikaj, D., Vaupotič, J., 2017. Parameters influencing deviation of radon concentration from its typical diurnal pattern in the winter and summer seasons. Geol. Maced. 31, 157–170.

Kikaj, D., Vaupotič, J., Chambers, S.D., 2019a. Identifying persistent temperature inversion events in a subalpine basin using radon-222. Atmos. Meas. Tech. 12 (8), 4455–4477.
Kikaj, D., Chambers, S.D., Vaupotič, J., 2019b. Radon-based atmospheric stability classification in contrasting sub-Alpine and sub-Mediterranean environments. J. Environ. Radioact. 203, 125–134. https://doi.org/10.1016/j.jenvrad.2019.03.010.
Kochowska, E., Kozak, K., Kozłowska, B., Mazur, J., 2009. Test measurements of thoron concentration using two ionization chambers AlphaGUARD vs radon monitor RAD7. Nukleonika 54, 189–192.
Largeron, Y., Staquet, C., 2016. Persistent inversion dynamics and wintertime PM_{10} air pollution in Alpine valleys. Atmos. Environ. 135, 92–108. https://doi.org/10.1016/j.atmosenv.2016.03.045.
Levin, I., Born, M., Cuntz, M., Langendörfer, U., Mantsch, S., Naegler, T., Schmidt, M., Varlagin, A., Verclas, S., Wagenbach, D., 2002. Observations of atmospheric variability and soil exhalation rate of radon-222 at a Russian forest site: Technical approach and deployment for boundary layer studies. Tellus Ser. B Chem. Phys. Meteorol. 54, 462–475. https://doi.org/10.1034/j.1600-0889.2002.01346.x.
Mazur, J., Kozak, K., 2014. Complementary system for long term measurements of radon exhalation rate from soil. Rev. Sci. Instrum. 85. https://doi.org/10.1063/1.4865156.
Moses, H., Stehney, A.F., Lucas Jr., H.F., 1960. The effect of meteorological variables upon the vertical and temporal distributions of atmospheric radon. J. Geophys. Res. 65, 1223–1238.
Perrino, C., Pietrodangelo, A., Febo, A., 2001. An atmospheric stability index based on radon progeny measurements for the evaluation of primary urban pollution. Atmos. Environ. 35, 5235–5244.
Petkovšek, Z., 1985. The termination of air pollution periods in valley basins. Zeitschrift für Meteorol. 35, 370–372.
Petkovšek, Z., 1992. Turbulent dissipation of cold air lake in a basin. Meteorog. Atmos. Phys. 47, 237–245. https://doi.org/10.1007/BF01025620.
Poberžnik, M., Štrumbelj, E., 2016. The effects of air mass transport, seasonality, and meteorology on pollutant levels at the Iskrba regional background station (1996 – 2014). Atmos. Environ. 134, 138–146. https://doi.org/10.1016/j.atmosenv.2016.03.059.
Podstawczyńska, A., Chambers, S.D., 2018. Radon-based technique for the analysis of atmospheric stability – a case study from Central Poland. Nukleonika 63, 47–54. https://doi.org/10.2478/nuka-2018-0006.
Pope, C.A., Dockery, D.W., 2006. Health effects of fine particulate air pollution: Lines that connect. J. Air Waste Manag. Assoc. 56, 709–742. https://doi.org/10.1080/10473289.2006.10464485.
Porstendörfer, J., Butterweck, G., Reineking, A., 1991. Diurnal variation of the concentrations of radon and its short-lived daughters in the atmosphere near the ground. Atmos. Environ. Part A, Gen. Top. 25, 709–713. https://doi.org/10.1016/0960-1686(91)90069-J.
Pucer, J., Štrumbelj, E., 2018. Impact of changes in climate on air pollution in Slovenia between 2002 and 2017. Environ. Pollut. 242, 398–406. https://doi.org/10.1016/j.envpol.2018.06.084.
Querol, X., Alastuey, A., Gangoiti, G., Perez, N., Lee, H.K., Eun, H.R., Park, Y., Mantilla, E., Escudero, M., Titos, G., Alonso, L., Temime-Roussel, B., Marchand, N., Moreta, J.R., Revuelta, M.A., Salvador, P., Artíñano, B., Dos Santos, S.G., Anguas, M., Notario, A., Saiz-Lopez, A., Harrison, R.M., Millán, M., Ahn, K.H., 2018. Phenomenology of summer ozone episodes over the Madrid Metropolitan Area. central Spain. Atmos. Chem. Phys. 18, 6511–6533. https://doi.org/10.5194/acp-18-6511-2018.
Rakovec, J., Merše, J., Jernej, S., Paradiž, B., 2002. Turbulent dissipation of the cold-air pool in a basin: Comparison of observed and simulated development. Meteorog. Atmos. Phys. 79, 195–213. https://doi.org/10.1007/s007030200003.
Rakovec, J., Skok, G., Žabkar, R., Žagar, N., 2015. The influence of the depth of a very shallow cool-pool lake on nocturnal cooling. Agric. For. Meteorol. 203, 17–29.
Sandradewi, J., Prévôt, A.S.H., Weingartner, E., Schmidhauser, R., Gysel, M., Baltensperger, U., 2008. A study of wood burning and traffic aerosols in an Alpine valley using a multi-wavelength Aethalometer. Atmos. Environ. 42, 101–112. https://doi.org/10.1016/j.atmosenv.2007.09.034.
Seinfeld, J.H., Pandis, S.N., 2006. Atmospheric Chemistry and Physics: From Air Pollution to Climate Change. John Willey & Sons Inc., New York.
Sesana, L., Caprioli, E., Marcazzan, G.M., 2003. Long period study of outdoor radon concentration in Milan and correlation between its temporal variations and dispersion properties of atmosphere. J. Environ. Radioact. 65, 147–160. https://doi.org/10.1016/S0265-931X(02)00093-0.
Sesana, L., Ottobrini, B., Polla, G., Facchini, U., 2006. ^{222}Rn as indicator of atmospheric turbulence: Measurements at Lake Maggiore and on the pre-Alps. J. Environ. Radioact. 86 (2), 271–288. https://doi.org/10.1016/j.jenvrad.2005.09.005.
Silcox, G.D., Kelly, K.E., Crosman, E.T., Whiteman, C.D., Allen, B.L., 2012. Wintertime $PM_{2.5}$ concentrations during persistent, multi-day cold-air pools in a mountain valley. Atmos. Environ. 46, 17–24. https://doi.org/10.1016/j.atmosenv.2011.10.041.
Sun, J., Birmili, W., Hermann, M., Tuch, T., Weinhold, K., Spindler, G., Schladitz, A., Bastian, S., Löschau, G., Cyrys, J., Gu, J., 2019. Variability of black carbon mass concentrations, sub-micrometer particle number concentrations and size distributions: results of the German Ultrafine Aerosol Network ranging from city street to high Alpine locations. Atmos. Environ. 202, 256–268.
Titos, G., Lyamani, H., Drinovec, L., Olmo, F.J., Močnik, G., Alados-Arboledas, L., 2015. Evaluation of the impact of transportation changes on air quality. Atmos. Environ. 114, 19–31. https://doi.org/10.1016/j.atmosenv.2015.05.027.
Uria-Tellaetxe, I., Carslaw, D.C., 2014. Conditional bivariate probability function for source identification. Environ. Model. Softw. 59, 1–9. https://doi.org/10.1016/j.envsoft.2014.05.002.
VanReken, T.M., Dhammapala, R.S., Jobson, B.T., Bottenus, C.L., VanderSchelden, G.S., Kaspari, S.D., Gao, Z., Zhu, Q., Lamb, B.K., Liu, H., Johnston, J., 2017. Role of persistent low-level clouds in mitigating air quality impacts of wintertime cold pool conditions. Atmos. Environ. 154, 236–246. https://doi.org/10.1016/j.atmosenv.2017.01.043.
Vrhovec, T., 1990. Analysis of mesometeorological temperature fields. Meteorog. Atmos. Phys. 43, 235–240.
Wang, F., Chambers, S.D., Zhang, Z., Williams, A.G., Deng, X., Zhang, H., Lonati, G., Crawford, J., Griffiths, A.D., Ianniello, A., Allegrini, I., 2016. Quantifying stability influences on air pollution in Lanzhou, China, using a radon-based "stability monitor": Seasonality and extreme events. Atmos. Environ. 145, 376–391. https://doi.org/10.1016/j.atmosenv.2016.11.003.
Wang, L., Stanič, S., Eichinger, W., Močnik, G., Drinovec, L., Gregorič, A., et al., 2019. Investigation of Aerosol Properties and Structures in Two Representative Meteorological Situations over the Vipava Valley Using Polarization Raman LiDAR. Atmosphere 10 (3), 128–140. https://www.mdpi.com/2073-4433/10/3/128.
Whiteman, C.D., 1982. Breakup of temperature inversions in deep mountain valleys: Part I. observations. J. Appl. Meteorol. https://doi.org/10.1175/1520-0450(1983)022 < 1314:COOTII > 2.0.CO;2.
Whiteman, C.D., Eisenbach, S., Pospichal, B., Steinacker, R., 2004. Comparison of vertical soundings and sidewall air temperature measurements in a small Alpine Basin. J. Appl. Meteorol. 43, 1635–1647. https://doi.org/10.1175/JAM2168.1.
Whiteman, C.D., Hoch, S.W., Horel, J.D., Charland, A., 2014. Relationship between particulate air pollution and meteorological variables in Utah's Salt Lake Valley. Atmos. Environ. 94, 742–753. https://doi.org/10.1016/j.atmosenv.2014.06.012.
Williams, A., Zahorowski, W., Chambers, S., Griffiths, A., 2011. The vertical distribution of radon in clear and cloudy daytime terrestrial boundary layers. J. Atmos. Sci. 68, 155–174. https://doi.org/10.1175/2010JAS3576.1.
Williams, A.G., Chambers, S., Griffiths, A., 2013. Bulk mixing and decoupling of the nocturnal stable boundary layer characterized using a ubiquitous natural tracer. Boundary-Layer Meteorol. 149, 381–402. https://doi.org/10.1007/s10546-013-9849-3.
Williams, A.G., Chambers, S.D., Conen, F., Reimann, S., Hill, M., Griffiths, A.D., Crawford, J., 2016. Radon as a tracer of atmospheric influences on traffic-related air pollution in a small inland city. Tellus, Ser. B Chem. Phys. Meteorol. 68, 1–21. https://doi.org/10.3402/tellusb.v68.30967.
Zahorowski, W., Chambers, S.D., Henderson-Sellers, A., 2004. Ground based radon-222 observations and their application to atmospheric studies. J. Environ. Radioact. 76, 3–33. https://doi.org/10.1016/j.jenvrad.2004.03.033.